Do we really need alternatives to the $\omega_0\omega_a$CDM parametrization after the DESI DR2?

Youri Carloni,[1,2,3,*] Orlando Luongo,[4,3,5,6,7,†] and Marek Biesiada[8,‡]

[1]*Università di Camerino, Divisione di Fisica, Via Madonna delle carceri 9, 62032 Camerino, Italy*
[2]*INFN, Sezione di Perugia, Perugia 06123, Italy*
[3]*INAF-Osservatorio Astronomico di Brera, Milano, Italy*
[4]*Università di Camerino, Via Madonna delle Carceri, Camerino 62032, Italy*
[5]*Istituto Nazionale di Fisica Nucleare, Sezione di Perugia, Perugia 06123, Italy*
[6]*SUNY Polytechnic Institute, Utica, New York 13502, USA*
[7]*Al-Farabi Kazakh National University, Al-Farabi Avenue 71, 050040 Almaty, Kazakhstan*
[8]*National Centre for Nuclear Research, Pasteura 7, 02-093 Warsaw, Poland*

(Received 8 August 2026; accepted 25 September 2026; published 10 November 2026)

We introduce a density-level pivot construction for the Chevallier–Polarski–Linder parametrization by defining the normalized dark energy density $f_p \equiv f(a_p)$ and the equation of state $\omega_p \equiv \omega(a_p)$ at an optimized pivot scale factor a_p. This reparametrization leaves the underlying cosmology unchanged and allows the two models to be compared using parameters with a direct physical interpretation at the epoch where the data are most sensitive. Accordingly, following the DESI DR2 results, we compare a newly proposed f_af_bCDM parametrization, based on a second-order Taylor expansion of the normalized dark energy density, with the standard $\omega_0\omega_a$CDM model. In particular, we constrain the original and pivoted parametrizations using the compressed cosmic microwave background, DESI DR2 baryon acoustic oscillations, cosmic chronometers, and Pantheon + Type Ia supernovae data, with the SH0ES prior imposed on H_0. We find that applying the same density-level pivot prescription to the $\omega_0\omega_a$CDM model substantially reduces the correlation between its dark energy parameters and provides less correlated constraints in the pivot variables. The statistical comparison shows that this model remains favored over the Taylor expansion of the dark energy density, even when both models are analyzed in the optimized parameter basis. Moreover, the pivoted Chevallier–Polarski–Linder parametrization accurately reproduces the background evolution of quintessence models, providing a reliable phenomenological approximation to the underlying dark energy dynamics, better than the f_af_bCDM model. We conclude that changing the parameter basis improves the performance of the $\omega_0\omega_a$CDM model, which emerges as the most suitable framework to describe the dark energy sector within the class of models considered here.

DOI: 10.1103/vrgg-2b2t

I. INTRODUCTION

The nature and fundamental properties of dark energy have acquired renewed interest after the possible evidence of its late time evolution [1–4]. The physical origin of the cosmic speedup remains one of the open challenges of modern cosmology, as it drives the Universe to accelerate with a repulsive [5,6] negative pressure [7–9].

Within the standard picture, the observed acceleration is described by a cosmological constant, Λ, whose equation of state is fixed to $\omega = -1$ [10–15]. This minimal paradigm has been considered for decades almost definitive since it passed several cosmological tests [16–24], being successful at the level of background expansion and large-scale structure, providing the reference against any dark energy sector, see, e.g., Refs. [25–35].

Conceptually, however, the physical origin of Λ remains unclear, being jeopardized by fine-tuning and coincidence issues [36–42], intimately related to the well-known *cosmological constant problem* [43–49] as well as recent cosmological tensions [50–55].

The recent baryon acoustic oscillations (BAO) measurements have provided unexpected evidence for evolving dark energy, departing from the standard ΛCDM model [56–60]. Even though Dark Energy Spectroscopic Instrument (DESI) results establish a departure from the

*Contact author: youri.carloni@unicam.it
†Contact author: orlando.luongo@unicam.it
‡Contact author: marek.biesiada@ncbj.gov.pl

Published by the American Physical Society under the terms of the Creative Commons Attribution 4.0 International license. Further distribution of this work must maintain attribution to the author(s) and the published article's title, journal citation, and DOI.

cosmological constant, the apparent preference for an evolving dark energy is not clearly robust under changes of parameter basis, priors, and theoretical representation of the same background dynamics, leaving open heated debates about the best dark energy form and its physical interpretation [61–68]. For example, criticisms have been raised against the evidence of dark energy evolution [69–74] and against the way the data have been analyzed [75–80].

To describe the effects of an evolving dark energy term, a widely used phenomenological description has been used under the form of the well-consolidated w_0w_aCDM model, originally presented as the Chevallier–Polarski–Linder (CPL) parametrization. There, dark energy's equation of state is written as a first order expansion in terms of the scale factor around the present time.

The original CPL formulation showed an evident and well-known correlation between the two parameters, ω_0 and ω_a, whose sum was supposed to be fixed to values typically larger than -1. The strong correlation still persists in the broader scenario offered by the w_0w_aCDM model, where however the two parameters are free to vary, and indeed, they have been bounded to behave phantom in several redshift domains[1] [56–58,81–83].

In this respect, the use of pivot variables appears quite interesting as a statistical landscape to reduce such a correlation [84–89]. In the standard construction, one introduces the value of the equation of state at a pivot scale factor, $\omega_p = \omega(a_p)$, where a_p is chosen so that ω_p is uncorrelated with the time variation parameter. Accordingly, the pivot parameter acquires a direct physical interpretation, i.e., the equation of state evaluated at the epoch where the data are most sensitive to dark energy dynamics. Thus, the pivot method replaces a highly correlated coordinate system in parameter space by a more suitable one, appearing as a sort of "phase-space coordinate change."

A direct application of the pivot method lies on using it with different dark energy models, checking the statistical most favored one. In this respect, a remarkable and recent alternative to the $\omega_0\omega_a$CDM model has been proposed at the level of the normalized dark energy density [88,90]. This consists of expanding the normalized dark energy function, $f(a)$, around the present epoch,[2] deriving a f_af_bCDM model, in analogy to CPL [81,83].

Motivated by the above reasons and in view of alternative dark energy parametrizations, we here wonder whether this apparent improvement, due to the pivot scale, appears as an intrinsic property of the density expansion or whether it is mainly a coordinate effect. Rephrasing it differently, if the CPL model is analyzed in the same physical basis used for the density parametrization, does the density expansion still retain a direct advantage, as DESI claimed? Accordingly, posterior degeneracies, contour shapes, and apparent parameter stability may depend strongly on the chosen coordinates. Hence, a model may look more constrained not because it is physically preferred but because it has been represented in a parameter basis more closely aligned with the directions actually measured by the data. We therefore apply the pivot technique to check whether the $\omega_0\omega_a$CDM parametrization appears favored or not, compared to alternatives, by switching the coordinate basis. To do so, we therefore apply a density-level pivot construction directly to the CPL parametrization. We define, for both CPL and f_af_bCDM scenarios, the pivot pair $(\omega_p, f_p) = (\omega(a_p), f(a_p))$, where a_p is chosen by minimizing the correlation between $\omega(a_p)$ and $f(a_p)$ over the posterior distribution. For the $\omega_0\omega_a$CDM model, the normalized dark energy density is fixed by the conservation equation once ω_0 and ω_a are specified.[3] Consequently, we raise at least two main consequences of our recipe: (1) the first is to understand which kind of expansion is favored, between expanding $\omega(a)$ and $f(a)$; (2) the second is the choice of coordinates used to represent the same posterior distribution. Indeed, by applying the same pivot logic to both parametrizations, we show that a significant part of the apparent advantage of the density-level expansion can be traced to the parameter basis and, therefore, not to the functional form itself. In particular, we find that once CPL is expressed in the pivoted variables (ω_p, f_p), its dark energy parameters become substantially less correlated and the corresponding constraints become more stable, being favored with respect to the parametrization made on the dark energy density. We then compare both parametrizations with a combination of compressed cosmic microwave background (CMB) information, DESI Data Release (DR2) BAO measurements, cosmic chronometers (CC) data, Pantheon + Type Ia supernovae, and the SH0ES prior on H_0. We find that the (ω_0, ω_a) parametrization remains statistically competitive, being mildly preferred over the density expansion in the dataset combination considered here. For completeness, our findings represent an effective phenomenological description of background expansion and may open avenues toward alternatives to the standard w_0w_aCDM scenario that can, conversely, be represented even in an alternative picture, namely, differently from the (ω_0, ω_a) basis. In addition, we compare the two pivoted

[1]Nevertheless, this correlation does not reflect a physical degeneracy of the dark energy sector itself, implying that the data constrain particular combinations of ω_0 and ω_a more accurately than the two original coefficients separately.

[2]This form automatically satisfies the normalization condition $f(1) = 1$ and allows the background evolution to be described directly in terms of the dark energy density. When combined with a density-level pivot construction, it can lead to compact and weakly correlated constraints in the parameter space.

[3]The transformation from (ω_0, ω_a) to (ω_p, f_p) is an exact reparametrization of the same cosmological model. For the density expansion, the same pivot variables can be constructed from the set (f_a, f_b). This allows the two models to be compared in a common physical coordinate system.

parametrizations with a canonical quintessence model driven by exponential and Ratra–Peebles inverse power-law potentials. We find that both parametrizations reproduce the corresponding Hubble history with high accuracy over the redshift range relevant for late time probes. Nevertheless, for the cases considered here, the pivoted CPL parametrization reaches a smaller maximum relative deviation and recovers more closely the physical dark energy quantities at the pivot epoch. This further supports the conclusion that the standard CPL form remains a robust and efficient approximation once the coordinate degeneracy of its original basis is removed and, at the same time, as stated above, does not preclude the search for alternative more suitable dark energy expansions.

The paper is structured as follows. In Sec. II, we review the standard pivot construction for the CPL parametrization and introduce the density-level pivot variables (ω_p, f_p). We then derive the explicit transformations connecting these variables to the original CPL parameters and to the coefficients of the $f_a f_b$CDM density expansion. In Sec. III, we describe the cosmological datasets and likelihoods used in the analysis, including compressed CMB information, DESI DR2 BAO measurements, cosmic chronometers, Pantheon + supernovae, and the SH0ES prior. We also present the Markov chain Monte Carlo (MCMC) constraints in both the original and pivoted parameter bases. In Sec. IV, we test the ability of the pivoted parametrizations to reconstruct the background expansion of exponential and Ratra–Peebles quintessence models and quantify the maximum relative deviation in the Hubble rate. Finally, in Sec. V, we summarize our results and discuss the implications of the coordinate dependence of dark energy constraints for future phenomenological analyses.

II. PIVOTING DARK ENERGY

The standard pivot procedure for the CPL parametrization,

$$\omega(a) = \omega_0 + \omega_a(1-a), \tag{1}$$

as discussed in Refs. [82,84,87], aims to remove the correlation between the parameters ω_0 and ω_a by introducing the pivot parameter,

$$\omega_p \equiv \omega(a_p) = \omega_0 + \omega_a(1-a_p), \tag{2}$$

where a_p denotes the pivot scale factor.

The latter is determined by requiring ω_p to be uncorrelated with ω_a, namely,

$$\langle \delta\omega_p \delta\omega_a \rangle = 0, \tag{3}$$

where the angular brackets denote statistical expectation values over the parameter distribution and $\delta\omega_i \equiv \omega_i - \langle \omega_i \rangle$, with $i = p, a$, so that $\langle \delta\omega_p \delta\omega_a \rangle$ represents the covariance between ω_p and ω_a.

Then, using the definition of ω_p, Eq. (3) yields

$$\langle \delta\omega_0 \delta\omega_a \rangle + (1-a_p)\langle \delta\omega_a^2 \rangle = 0, \tag{4}$$

from which the pivot scale factor follows as

$$a_p = 1 + \frac{\langle \delta\omega_0 \delta\omega_a \rangle}{\langle \delta\omega_a^2 \rangle}. \tag{5}$$

Although this standard pivot construction successfully removes the correlation between the equation of state parameters, it still relates a physically meaningful quantity, namely, the equation of state evaluated at the pivot redshift, ω_p to the purely geometrical parameter ω_a, which only describes the variation of the equation of state around the present epoch. Motivated by the search for a more physically interpretable parameter basis, Ref. [88] introduced an alternative pivot approach directly at the dark energy density-level.

Instead of expanding the equation of state, the normalized dark energy density is parametrized through a second order Taylor expansion around the present epoch, named $f_a f_b$CDM, that is given by

$$f(a) \equiv \frac{\rho_{\rm DE}(a)}{\rho_{\rm DE,0}} = 1 + f_a(1-a) + f_b(1-a)^2, \tag{6}$$

where f_a and f_b control the linear and quadratic terms of the normalized dark energy density expansion around $a = 1$, with $f_a = -f'(1)$ and $f_b = f''(1)/2$. This parametrization automatically satisfies the normalization condition, i.e., $f(1) = 1$, and provides a direct description of the background dynamics in terms of the energy density itself.

Here, by applying the conservation equation,

$$\frac{d\ln\rho_{\rm DE}}{d\ln a} = -3[1+\omega(a)], \tag{7}$$

we can reconstruct the corresponding equation of state as

$$\omega(a) = -1 + \frac{a[f_a + 2f_b(1-a)]}{3f(a)}. \tag{8}$$

In contrast to the previous pivot method, the density-level expansion naturally leads to the definition of the pivot pair (ω_p, f_p), where $f_p \equiv f(a_p)$ and $f(a)$ is defined in Eq. (6). Both quantities have a direct physical interpretation, representing, respectively, the dark energy equation of state and the normalized dark energy density evaluated at the pivot epoch.

This construction substantially reduces parameter degeneracies while preserving a connection with the underlying dark energy dynamics.

The method appears to favor the $f_a f_b$CDM over the conventional $\omega_0\omega_a$CDM parametrization. This observation

motivates a more detailed investigation of the origin of such an improvement.

Indeed, the pivot procedure introduced in Ref. [88] was specifically developed for the density-level expansion. However, from a purely methodological perspective, there is no fundamental reason preventing a similar construction from being applied to the standard CPL parametrization. Since the pivot technique is designed to provide a physically meaningful parameter basis with reduced correlations, it is natural to explore whether an analogous density pivot approach can be formulated directly within the $\omega_0\omega_a$CDM framework.

For this reason, we generalize the density-level pivot formalism to the CPL model and compare its performance against the alternative f_af_bCDM parametrization.

With this aim, we express both the models in terms of the physically motivated pivot pair (ω_p, f_p). For the CPL parametrization, the normalized dark energy density is

$$f(a) = a^{-3(1+\omega_0+\omega_a)} e^{3\omega_a(a-1)}, \tag{9}$$

then the original CPL parameters (ω_0, ω_a) can be reconstructed from (ω_p, f_p) as

$$\omega_a = \frac{\ln f_p + 3(1+\omega_p)\ln a_p}{3[(a_p-1) - a_p \ln a_p]}, \tag{10}$$

and

$$\omega_0 = \omega_p - (1-a_p)\omega_a. \tag{11}$$

Instead, for the density-level parametrization given by Eq. (6), the relation between (f_a, f_b) and (ω_p, f_p) is provided by

$$f_a = \frac{2(f_p-1)}{1-a_p} - \frac{3f_p(1+\omega_p)}{a_p}, \tag{12}$$

and

$$f_b = \frac{3f_p(1+\omega_p)\frac{1-a_p}{a_p} - f_p + 1}{(1-a_p)^2}. \tag{13}$$

This allows us to disentangle the effect of the pivot transformation itself from the specific choice of the dark energy parametrization, providing a more direct assessment of the origin of the observed reduction in parameter degeneracies.

The pivot construction does not modify the underlying cosmological model. Indeed, the expansion history, the dark energy density evolution, the equation of state, and the likelihood function remain unchanged. The procedure introduces a new coordinate system in parameter space, replacing the highly correlated expansion coefficients by two quantities with a direct physical interpretation, i.e., the dark energy density and equation of state evaluated at the pivot epoch.

III. DATA ANALYSIS

We perform the MCMC analysis through MontePython[4] by combining the following probes from early to late times.

A. Compressed CMB

We include CMB information through the compressed likelihood adopted in Refs. [57,88], which contains the geometrical early-Universe constraints relevant for the present background-level analysis. Here, we consider the parameter vector,

$$\mathbf{X}_{\rm CMB} = (\theta_\star, \omega_b, \omega_{bc}), \tag{14}$$

where $\theta_\star$ denotes the angular size of the sound horizon at photon decoupling, $\omega_b = \Omega_b h^2$ is the physical baryon density, and

$$\omega_{bc} = (\Omega_b + \Omega_{\rm cdm})h^2 \tag{15}$$

is the total physical baryon plus cold-dark-matter density. The physical matter densities primarily constrain the prerecombination physics and calibrate the sound-horizon scale, while $\theta_\star$ also contains geometrical information through the distance to last scattering.

The compressed CMB is then implemented through a multivariate Gaussian prior with mean vector,

$$\mathbf{X}_{\rm obs} = (0.0104110, 0.02223, 0.14208), \tag{16}$$

and covariance matrix,

$$\mathbf{C} = 10^{-9}\begin{pmatrix} 0.006621 & 0.12444 & -1.1929 \\ 0.12444 & 21.344 & -94.001 \\ -1.1929 & -94.001 & 1488.4 \end{pmatrix}. \tag{17}$$

Finally, the compressed CMB log-likelihood, denoted as QCMB, can be written as

$$\ln \mathcal{L}_{\rm QCMB} \propto -\frac{1}{2}\Delta\mathbf{X}^T\mathbf{C}^{-1}\Delta\mathbf{X}, \tag{18}$$

where $\Delta\mathbf{X} = \mathbf{X}_{\rm obs} - \mathbf{X}_{\rm th}$.

In the present analysis, the CMB information is included through the compressed likelihood defined above, which retains the main geometrical constraints relevant for the background evolution, namely, the physical matter densities and the angular acoustic scale $\theta_\star$. This differs from a full CMB likelihood, which uses the temperature and polarization power spectra, together with CMB lensing, and therefore contains additional information beyond the

[4] https://github.com/brinckmann/montepython_public.

TABLE I. The DESI DR2 BAO dataset adopted in this analysis. The table reports the tracer sample, the corresponding effective redshift $z_{\rm eff}$, and the measured BAO observables with their associated 1σ errors. The tracers include the Bright Galaxy Survey (BGS), luminous red galaxies (LRG), emission-line galaxies (ELG), quasi-stellar objects (QSO), the Lyman-alpha forest– quasar sample (Lyα QSO), and the combined LRG + ELG sample.

Tracer	$z_{\rm eff}$	D_M/r_d	D_H/r_d	D_V/r_d
BGS	0.295	⋯	⋯	7.942 ± 0.075
LRG1	0.510	13.588 ± 0.167	21.863 ± 0.425	⋯
LRG2	0.706	17.351 ± 0.177	19.455 ± 0.330	⋯
LRG3+ ELG1	0.934	21.576 ± 0.152	17.641 ± 0.193	⋯
ELG2	1.321	27.601 ± 0.318	14.176 ± 0.221	⋯
QSO	1.484	30.512 ± 0.760	12.817 ± 0.516	⋯
Lyα QSO	2.330	38.988 ± 0.531	8.632 ± 0.101	⋯

purely geometrical constraints encoded in QCMB. The two approaches are thus sensitive to partly different aspects of the cosmological model, while the compressed likelihood is particularly suited to the background-level comparison performed here.

B. DESI DR2

The baryon acoustic oscillation measurements considered in this work are taken from the second DESI data release [57]. This sample provides constraints on several distance indicators, i.e., the transverse comoving distance,

$$\frac{D_{\rm M}(z)}{r_{\rm d}} = \frac{c}{r_{\rm d}} \int_0^z \frac{dz'}{H(z')}, \tag{19}$$

the line-of-sight distance,

$$\frac{D_{\rm H}(z)}{r_{\rm d}} = \frac{c}{r_{\rm d} H(z)}, \tag{20}$$

and the spherically averaged distance,

$$\frac{D_{\rm V}(z)}{r_{\rm d}} = \frac{[z D_{\rm H}(z) D_{\rm M}^2(z)]^{1/3}}{r_{\rm d}}. \tag{21}$$

These observations cover the redshift range $0.295 \leq z \leq 2.33$, and we include the 13 correlated BAO measurements summarized in Table I.

At this point, the DESI log-likelihood can be written as

$$\ln \mathcal{L}_{\rm DESI} \propto -\frac{1}{2} \Delta \mathbf{Y}^T \mathbf{C}^{-1} \Delta \mathbf{Y}, \tag{22}$$

where

$$\Delta \mathbf{Y} = \mathbf{Y}_{\rm obs} - \mathbf{Y}_{\rm th}, \tag{23}$$

with $\mathbf{Y}_{\rm obs}$ representing the DESI DR2 measurements, while $\mathbf{Y}_{\rm th}$ contains the corresponding theoretical predictions,

$$\mathbf{Y} \in \{D_M(z)/r_d, D_H(z)/r_d, D_V(z)/r_d\}, \tag{24}$$

evaluated at the effective redshifts of the survey. The covariance matrix $\mathbf{C}$ associated with the DESI DR2 BAO data is publicly available through the MontePython repository [91].

C. CC 2016

We consider the 32 CC 2016 measurements of the Hubble parameter spanning the redshift range $z \in [0.07, 1.965]$, reported in Table II. Although these measurements are affected by relatively large observational uncertainties, they provide a direct and largely model-independent determination of the cosmic expansion rate [92].

TABLE II. Compilation of the CC data employed in this work, including the redshift measurements, the corresponding Hubble parameter determinations $H(z)$ with uncertainties, and the relevant bibliographic references.

z	$H(z)$ $(\mathrm{km\,s^{-1}\,Mpc^{-1}})$	References
0.07	69.0 ± 19.6	[93]
0.09	69.0 ± 12.0	[92]
0.12	68.6 ± 26.2	[93]
0.17	83.0 ± 8.0	[94]
0.179	75.0 ± 4.0	[95]
0.199	75.0 ± 5.0	[95]
0.20	72.9 ± 29.6	[93]
0.27	77.0 ± 14.0	[94]
0.28	88.8 ± 36.6	[93]
0.352	83.0 ± 14.0	[96]
0.38	83.0 ± 13.5	[96]
0.4	95.0 ± 17.0	[94]
0.4004	77.0 ± 10.2	[96]
0.425	87.1 ± 11.2	[96]
0.445	92.8 ± 12.9	[96]
0.47	89.0 ± 23.0	[97]
0.4783	80.9 ± 9.0	[96]
0.48	97.0 ± 62.0	[98]
0.593	104.0 ± 13.0	[95]
0.68	92.0 ± 8.0	[95]
0.75	98.8 ± 33.6	[99]
0.781	105.0 ± 12.0	[95]
0.875	125.0 ± 17.0	[95]
0.88	90.0 ± 40.0	[98]
0.9	117.0 ± 23.0	[94]
1.037	154.0 ± 20.0	[95]
1.3	168.0 ± 17.0	[94]
1.363	160.0 ± 33.6	[100]
1.43	177.0 ± 18.0	[94]
1.53	140.0 ± 14.0	[94]
1.75	202.0 ± 40.0	[94]
1.965	186.5 ± 50.4	[100]

The CC technique is based on passively evolving galaxies, whose differential age evolution can be used to estimate the Hubble parameter through

$$H(z) = -\frac{1}{1+z}\frac{\Delta z}{\Delta t}. \tag{25}$$

Assuming independent Gaussian measurements, the corresponding log-likelihood is given by

$$\ln \mathcal{L}_{\rm CC} \propto -\frac{1}{2}\sum_i \left[\frac{H_i - H(z_i)}{\sigma_{H_i}}\right]^2, \tag{26}$$

where H_i denotes the observed Hubble parameter at redshift z_i, $H(z_i)$ is the theoretical prediction of the cosmological model, and σ_{H_i} represents the associated observational uncertainty.

D. Pantheon+ and SH0ES prior

We employ the Pantheon + compilation [31], consisting of 1701 light curves from 1550 distinct Type Ia supernovae spanning the redshift range $0.001 < z < 2.26$. Following the adopted Pantheon + likelihood implementation, only supernovae with $z > 0.01$ are included in the likelihood.

The corresponding theoretical distance modulus is

$$\mu_{\rm th}(z) = 5\log_{10}\left(\frac{D_L(z)}{\rm Mpc}\right) + 25, \tag{27}$$

where

$$D_L(z) = c(1+z)\int_0^z \frac{dz'}{H(z')} \tag{28}$$

denotes the luminosity distance predicted by the cosmological model assuming a flat Universe.

The Pantheon+ log-likelihood then can be written as

$$\ln \mathcal{L}_{\rm PP} \propto -\frac{1}{2}\Delta\boldsymbol{\mu}^T \mathbf{C}^{-1}\Delta\boldsymbol{\mu}, \tag{29}$$

where

$$\Delta\boldsymbol{\mu} = \boldsymbol{\mu}_{\rm obs} - \boldsymbol{\mu}_{\rm th}. \tag{30}$$

Here, $\boldsymbol{\mu}_{\rm obs}$ and $\boldsymbol{\mu}_{\rm th}$ denote the observed and theoretical distance moduli, respectively, while $\mathbf{C}$ is the full covariance matrix supplied by the Pantheon + Collaboration.

We also consider the SH0ES determination [101],

$$H_0 = 73.04 \pm 1.04\ {\rm km\,s^{-1}\,Mpc^{-1}}, \tag{31}$$

as an independent Gaussian prior.

Thus, combining the information provided by the QCMB likelihood, DESI DR2 BAO measurements, CC data, the Pantheon + sample, and the SH0ES prior on the Hubble constant, the total log-likelihood adopted in this work is given by

$$\ln \mathcal{L} = \ln \mathcal{L}_{\rm QCMB} + \ln \mathcal{L}_{\rm DESI} + \ln \mathcal{L}_{\rm CC} + \ln \mathcal{L}_{\rm PP} + \ln \mathcal{L}_{\rm SH0ES}. \tag{32}$$

Then, the resulting posterior distributions are explored through a MCMC analysis, from which the cosmological constraints and confidence intervals are derived.

E. Numerical results

We first perform separate MCMC analyses for the $\omega_0\omega_a$CDM and f_af_bCDM models in order to assess their relative statistical performance. The resulting posterior distributions are then used to determine the pivot scale factor associated with each parametrization.

To construct a physically motivated pivot representation of the dark energy density, we evaluate the quantities ω_p and f_p for each sample of the posterior distributions obtained in the original parameter bases.

We define the pivot scale factor as the epoch at which ω_p and f_p are least correlated. Accordingly, a_p is determined by the condition

$$|{\rm corr}[\omega(a_p), f(a_p)]| = \min_a |{\rm corr}[\omega(a), f(a)]|, \tag{33}$$

where correlation is computed from the MCMC chains using the corresponding statistical weights and is defined as

$${\rm corr}(\omega, f) = \frac{\langle \delta\omega\delta f\rangle}{\sqrt{\langle(\delta\omega)^2\rangle\langle(\delta f)^2\rangle}}. \tag{34}$$

If the correlation crosses zero, this procedure yields an exactly decorrelated parameter basis; otherwise, it identifies the scale factor at which the residual correlation is minimized.

The flat priors adopted for the CPL model are $\omega_0 \in [-3, 1]$ and $\omega_a \in [-3, 1]$ while for the f_af_bCDM parametrization we consider $f_a \in [-1, 1]$ and $f_b \in [-1, 2]$. In the latter case, the parameter space is restricted by requiring the positivity of the normalized dark energy density, see Fig. 1, whereas no such restriction is needed for the CPL parametrization.

The numerical results are summarized in Table III, while the marginalized posterior distributions are shown in Figs. 2 and 3.

In this analysis, even after including the SH0ES prior on H_0, the Hubble tension persists, since the dark energy parametrizations considered in this work do not provide a viable late time solution to the tension [102–105].

To compare the statistical performance of the CPL and f_af_bCDM parametrizations, we employ the Akaike Information Criterion (AIC) and the Deviance Information Criterion (DIC) [106–110]. These criteria, accounting for

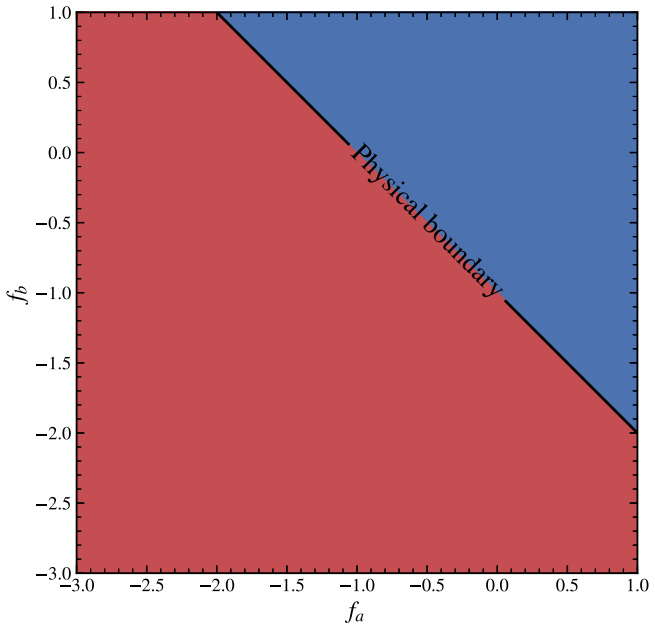


FIG. 1. Positivity regions in the (f_a, f_b) parameter space for the normalized dark energy density. The red region identifies parameter combinations for which $f(a) < 0$ for at least one value of the scale factor $a \in [0, 1]$, whereas the blue region indicates where the $f_a f_b$CDM model satisfies $f(a) > 0$ over the entire interval. The solid black curve marks the boundary $\min_{a\in[0,1]} f(a) = 0$ separating the physical and nonphysical regions.

both the quality of the fit and the complexity of the model, are defined as

$$\mathrm{AIC} = -2\ln\mathcal{L}_{\max} + 2k, \tag{35a}$$

$$\mathrm{DIC} = -2\ln\mathcal{L}_{\max} + 2p_{\mathrm{D}}, \tag{35b}$$

where $\mathcal{L}_{\max}$ is the maximum likelihood, k denotes the number of free parameters, and

TABLE III. Mean values of the cosmological parameters with their 1σ (2σ) uncertainties for the $\omega_0\omega_a$CDM and $f_a f_b$CDM parametrizations. For f_b, the constraint indicates the upper bound at 95% confidence level, since the posterior extends to the lower prior boundary. The minimum chi-square values are computed as $\chi^2_{\min} = -2\ln\mathcal{L}_{\max}$.

Parameter	$\omega_0\omega_a$CDM	$f_a f_b$CDM
$H_0(\mathrm{km\,s^{-1}\,Mpc^{-1}})$	$68.51^{+0.20(0.40)}_{-0.20(0.40)}$	$68.61^{+0.19(0.38)}_{-0.19(0.38)}$
Ω_{m}	$0.2995^{+0.0030(0.0059)}_{-0.0029(0.0058)}$	$0.2967^{+0.0026(0.0051)}_{-0.0026(0.0053)}$
ω_0	$-0.886^{+0.049(0.101)}_{-0.052(0.100)}$	⋯
ω_a	$-0.604^{+0.242(0.452)}_{-0.217(0.460)}$	⋯
f_a	⋯	$0.201^{+0.122(0.177)}_{-0.062(0.215)}$
f_b	⋯	< -0.24
$\chi^2_{\min}$	1464.98	1467.30

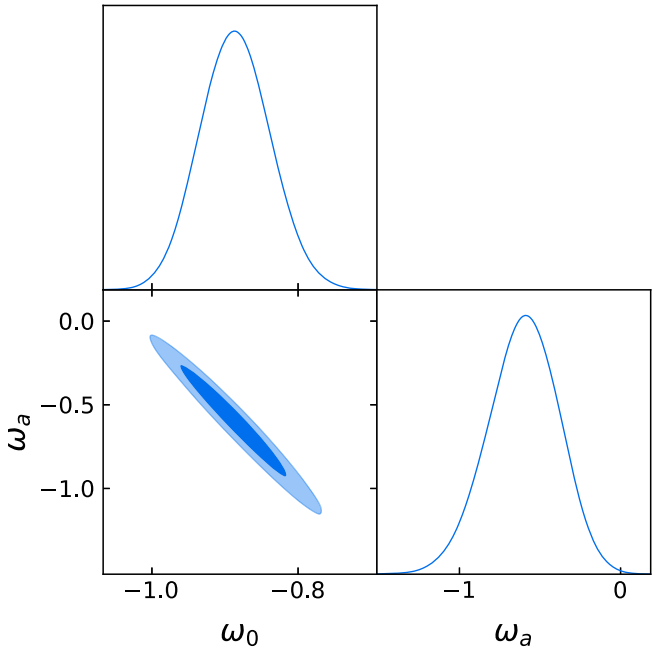


FIG. 2. Posterior for the $\omega_0\omega_a$CDM model obtained by combining compressed CMB, DESI DR2, CC, and Pantheon + data with the SH0ES prior on H_0.

$$p_{\mathrm{D}} = \langle -2\ln\mathcal{L}\rangle + 2\ln\mathcal{L}_{\max} \tag{36}$$

is the Bayesian complexity, namely, the effective number of parameters constrained by the data. While the AIC penalizes a model according to its total number of free parameters, the DIC replaces this quantity with p_{D} and therefore

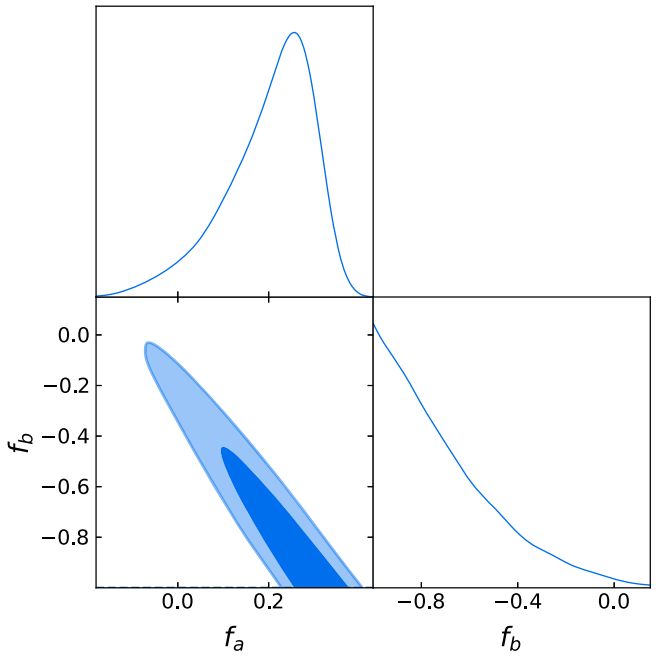


FIG. 3. Posterior for the $f_a f_b$CDM model obtained by combining compressed CMB, DESI DR2, CC, and Pantheon + data with the SH0ES prior on H_0.

accounts for the extent to which the parameters are effectively constrained by the posterior distribution.

Since the absolute values of these estimators do not carry a direct statistical interpretation, model comparison is performed through

$$\Delta X_i = X_i - X_{\rm ref}, \qquad X \in \{\mathrm{AIC}, \mathrm{DIC}\}, \tag{37}$$

where $X_{\rm ref}$ denotes the value obtained for the reference model. In the following, we take the $\omega_0\omega_a$CDM model as the reference, so that positive values of ΔX favor the reference model and negative values favor the model under consideration.

Using the above definitions, we can evaluate the differences ΔAIC and ΔDIC with respect to the reference scenario. These quantities provide a criterion to assess whether the improvement in the fit justifies the introduction of additional free parameters.

For positive values of ΔAIC or ΔDIC, the usual qualitative interpretation is as follows:

- $0 \leq \Delta\mathrm{AIC}(\Delta\mathrm{DIC}) \leq 2$ corresponds to weak evidence in favor of the reference scenario, so that no firm statistical preference can be assigned to either model;
- $2 < \Delta\mathrm{AIC}(\Delta\mathrm{DIC}) \leq 6$ indicates moderate evidence against the model under consideration;
- $\Delta\mathrm{AIC}(\Delta\mathrm{DIC}) > 6$ provides strong evidence against the model under consideration, suggesting that it is disfavored with respect to the reference scenario.

Hence, for the $\omega_0\omega_a$CDM and f_af_bCDM parametrizations, we obtain respectively,

$$\mathrm{AIC} = 1468.99, \qquad \mathrm{DIC} = 1474.99, \tag{38a}$$

$$\mathrm{AIC} = 1471.30, \qquad \mathrm{DIC} = 1477.74. \tag{38b}$$

Taking CPL as the reference model, these values correspond to

$$\Delta\mathrm{AIC}_{f_af_b\mathrm{CDM}} = 2.31, \qquad \Delta\mathrm{DIC}_{f_af_b\mathrm{CDM}} = 2.75, \tag{39}$$

indicating a modest preference for the CPL parametrization.

Then, we use the MCMC chains obtained from these analyses to determine the optimal pivot scale for both models.

For the density-level pivot representation of the CPL model, the condition $\mathrm{corr}(\omega_p, f_p) = 0$ admits two solutions within the investigated range of scale factors. We select the solution closest to the standard CPL pivot with CMB, DESI and Pantheon Plus data reported in Ref. [87], $z_p \simeq 0.26$, obtaining

$$a_p \simeq 0.76, \qquad z_p \simeq 0.31, \tag{40}$$

values apparently very close to the matter-dark energy equivalence [111–113] and not far from the transition time [114–117].

At this scale, the residual correlation is numerically consistent with zero,

$$\mathrm{corr}(\omega_p, f_p) \simeq 0, \tag{41}$$

showing that the transformation provides an effectively decorrelated parameter basis.

Applying the same minimization procedure to the f_af_bCDM parametrization, we find

$$a_p \simeq 0.71, \qquad z_p \simeq 0.42, \tag{42}$$

with

$$\mathrm{corr}(\omega_p, f_p) \simeq 0.13. \tag{43}$$

In this case, the correlation does not cross zero over the explored interval, and the deduced pivot therefore corresponds to the global minimum of $|\mathrm{corr}(\omega_p, f_p)|$. Although an exactly decorrelated basis cannot be obtained, the pivot transformation substantially reduces the degeneracy relative to the original (f_a, f_b) basis, for which

$$\mathrm{corr}(f_a, f_b) \simeq -0.93. \tag{44}$$

The absolute correlation is therefore reduced by approximately a factor of 7.3. The density-level pivot construction is thus more effective for the CPL model, where an exactly decorrelated basis can be identified, whereas in the f_af_bCDM case a nonvanishing residual correlation remains.

After fixing the pivot scale factors from the weighted chains in the original parameter bases, we perform new MCMC analyses in which (ω_p, f_p) are sampled directly with flat priors. These pivoted chains are therefore not obtained by transforming or reweighting the original chains.

Here, the MCMC results are summarized in Table IV, while the contour plots for both models obtained after the application of the pivot method are presented in Fig. 4.

TABLE IV. Mean values of the cosmological parameters with their 1σ (2σ) uncertainties for the pivoted $\omega_0\omega_a$CDM and f_af_bCDM parametrizations. The quantities ω_p and f_p denote the dark energy equation of state and normalized dark energy density evaluated at the corresponding pivot scale, respectively. The minimum chi-square values are the same as in Table III.

Parameter	$\omega_0\omega_a$CDM	f_af_bCDM
$H_0(\mathrm{km\,s^{-1}\,Mpc^{-1}})$	$68.51^{+0.19(0.39)}_{-0.20(0.38)}$	$68.57^{+0.19(0.38)}_{-0.19(0.38)}$
$\Omega_{\rm m}$	$0.2995^{+0.0029(0.0057)}_{-0.0028(0.0057)}$	$0.2978^{+0.0028(0.0054)}_{-0.0026(0.0054)}$
ω_p	$-1.031^{+0.012(0.024)}_{-0.011(0.024)}$	$-1.064^{+0.013(0.037)}_{-0.022(0.032)}$
f_p	$1.033^{+0.018(0.038)}_{-0.019(0.037)}$	$1.008^{+0.016(0.030)}_{-0.015(0.031)}$
$\chi^2_{\rm min}$	1464.98	1467.30

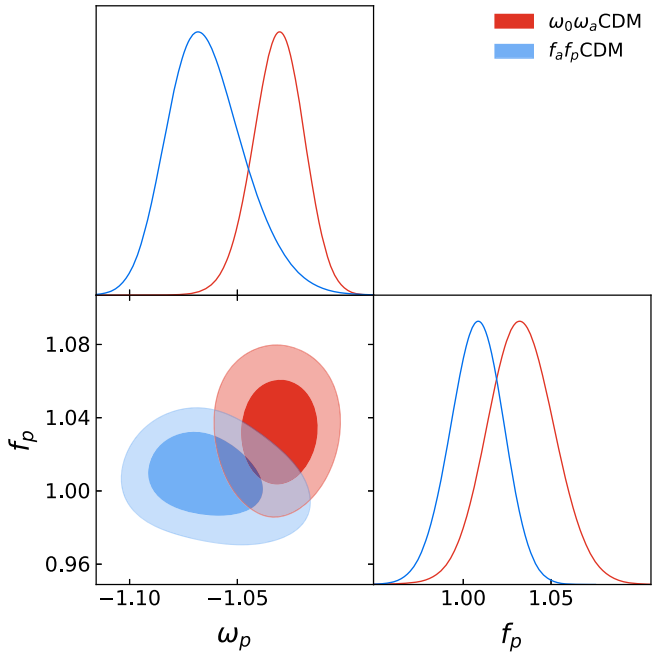


FIG. 4. Posteriors for the $\omega_0\omega_a$CDM and f_af_bCDM models after applying the pivot method. Contours are derived from the combination of compressed CMB, DESI DR2, CC, and Pantheon + data, together with the SH0ES prior on H_0.

IV. COMPARISON WITH QUINTESSENCE AFTER PIVOTING

In this section, we perform a reconstruction test that is conceptually distinct from the observational MCMC analysis of Sec. III. We examine how accurately the two parametrizations reproduce the background evolution of canonical quintessence models, while keeping the observationally determined pivot epochs fixed.

We consider a minimally coupled scalar field ϕ evolving in a spatially flat Friedmann–Lemaître–Robertson–Walker (FLRW) background, with energy density and pressure,

$$\rho_\phi = \frac{1}{2}\dot{\phi}^2 + V(\phi), \tag{45}$$

$$p_\phi = \frac{1}{2}\dot{\phi}^2 - V(\phi). \tag{46}$$

Its equation of state is therefore

$$\omega_\phi = \frac{\dot{\phi}^2/2 - V(\phi)}{\dot{\phi}^2/2 + V(\phi)}. \tag{47}$$

To test the two phenomenological parametrizations against different scalar field evolutions, we consider two well-known quintessence potentials,

$$V_{\rm exp}(\phi) = V_0 e^{\lambda\phi/M_{\rm Pl}}, \tag{48a}$$

$$V_{\rm RP}(\phi) = V_0\left(\frac{\phi}{M_{\rm Pl}}\right)^{-n}, \tag{48b}$$

where $M_{\rm Pl} = (8\pi G)^{-1/2}$ is the reduced Planck mass, and V_0 fixes the overall energy scale of each potential.

For the exponential potential, we select initial conditions corresponding to a thawing evolution [118,119]. At early times, the large Hubble friction keeps the field nearly frozen, so that its kinetic energy is negligible and $\omega_\phi \simeq -1$. As the expansion rate decreases, the field begins to roll, and its equation of state moves away from -1. With the sign convention adopted in Eq. (48) and $\lambda > 0$, the potential increases with ϕ, and the field rolls toward smaller values of ϕ. The exponential form can also admit other dynamical solutions for different slopes and initial conditions. Therefore, the thawing behavior refers here to the particular branch selected in our numerical implementation rather than to the potential alone [120,121].

We study the exponential potential behavior over the set

$$\lambda = \{0.3, 0.5, 0.7, 0.9, 1.1, 1.3, 1.4, 1.5\}. \tag{49}$$

The lower part of this interval probes slowly evolving models close to the constant-potential limit $\lambda = 0$, while larger values correspond to a steeper potential and lead to a more rapid evolution of the scalar field at late times. For the scalar field dominated exponential attractor, accelerated expansion requires $\lambda^2 < 2$ [120]. The upper part of our grid covers this characteristic scale. Indeed, $\lambda = 1.4$ lies close to $\sqrt{2}$, while $\lambda = 1.5$ tests a slightly steeper potential. This asymptotic condition does not exclude transient acceleration in the thawing solutions studied here, whose present evolution also depends on the initial conditions.

As a representative exponential example, we choose $\lambda = 0.7$. This value is sufficiently far from the constant-potential limit to produce a visible but moderate thawing evolution, while remaining well below $\lambda = \sqrt{2}$. It also coincides with the benchmark used in Refs. [88,122], allowing a direct comparison with previous quintessence reconstructions.

Then, we consider the inverse power-law potential introduced by Ratra and Peebles [123].

The form used in Eq. (48b) is equivalent to the conventional expression

$$V_{\rm RP}(\phi) = \frac{M^{4+n}}{\phi^n}, \tag{50}$$

provided that

$$V_0 = \frac{M^{4+n}}{M_{\rm Pl}^n}. \tag{51}$$

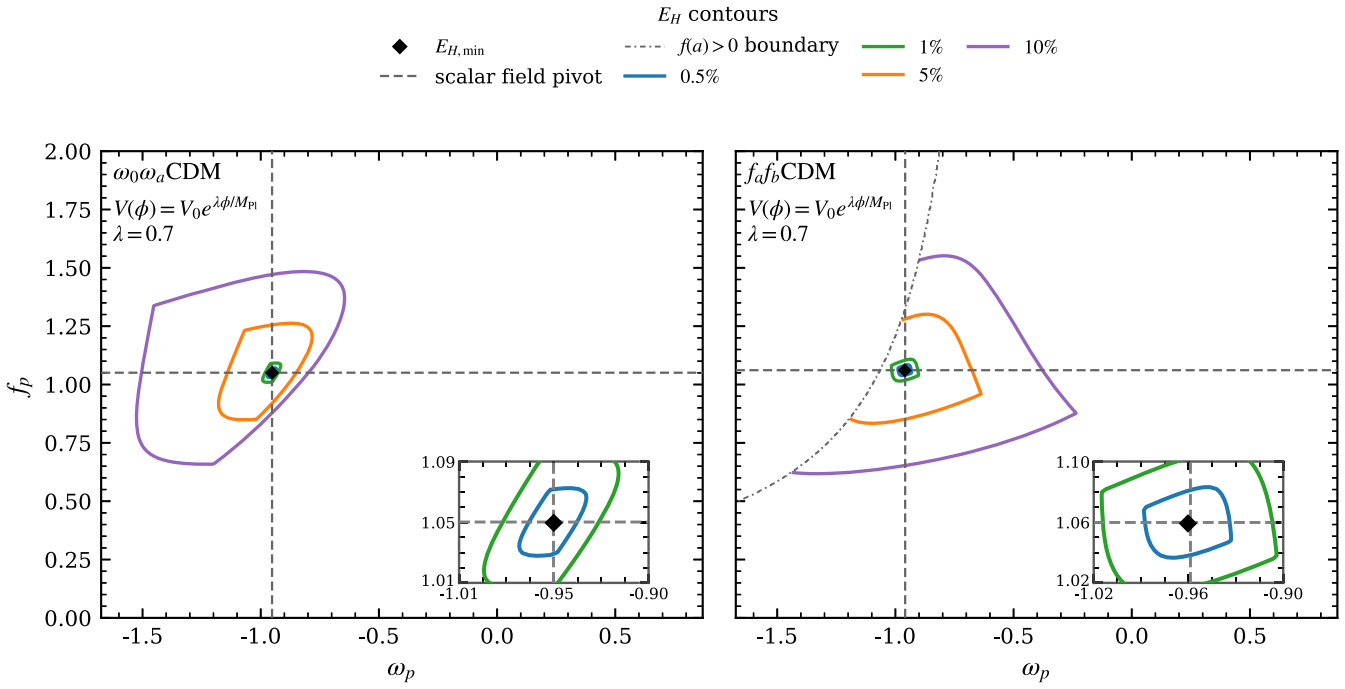


FIG. 5. Contours of the maximum relative Hubble rate error E_H, defined in Eq. (55), for the exponential quintessence potential $V(\phi) = V_0 e^{\lambda\phi/M_{\rm Pl}}$ with $\lambda = 0.7$. The left panel shows the reconstruction obtained with the pivoted $\omega_0\omega_a$CDM parametrization, whereas the right panel shows the corresponding result for f_af_bCDM. The contours correspond to $E_H = 0.5\%$, 1%, 5%, and 10%, as indicated in the legend. The black diamonds mark the continuously optimized minima $E_{H,\min}$, while the dashed gray lines indicate the exact values of $\omega_\phi(a_p)$ and $f_\phi(a_p)$ obtained from the scalar field solution at the pivot epoch of each parametrization. The insets show an enlarged view of the minimum error regions. In the f_af_bCDM panel, the gray dot-dashed line marks the boundary of the globally physical domain satisfying $f(a) > 0$ for every $0 < a \leq 1$.

Thus, the two expressions differ only in the definition of the normalization scale, and we use Eq. (48b) throughout the analysis.

For $n > 0$, the Ratra–Peebles potential decreases and becomes progressively flatter as ϕ increases. It admits attractorlike tracker solutions whose late time evolution is commonly associated with the freezing class of quintessence [118,124]. Along this type of trajectory, the scalar field evolves during the radiation- and matter-dominated eras with reduced sensitivity to its initial conditions. When the scalar field becomes dynamically significant, its equation of state evolves toward $\omega_\phi = -1$.

For an inverse power-law potential, the tracker equation of state during an epoch dominated by a background fluid with equation of state ω_B is given by [38,123,124],

$$\omega_{\phi,\rm tr} \simeq \frac{n\omega_B - 2}{n+2}. \tag{52}$$

During matter domination, $\omega_B = 0$, and this expression reduces to

$$\omega_{\phi,\rm tr} \simeq -\frac{2}{n+2}, \tag{53}$$

showing that larger values of n correspond to a larger departure from $\omega_\phi = -1$ [124]. Here, we explore the set

$$n = \{0.3, 0.5, 0.7, 0.9, 1.1, 1.3, 1.5, 1.7\}, \tag{54}$$

which spans shallow to moderately steep inverse power-law potentials. The lower end remains close to the constant potential limit $n = 0$, whereas the upper end probes more pronounced tracker dynamics without extending to very steep inverse power laws.

We display $n = 0.9$ since it lies near the center of the sampled interval and close to the commonly studied case $n = 1$. It yields a clear yet moderate departure from ΛCDM, making it a useful representative model for comparing the two reconstruction schemes.

The scalar field backgrounds are computed using the Cosmic Linear Anisotropy Solving System (CLASS) Boltzmann code.[5]

The representative cases $\lambda = 0.7$ and $n = 0.9$ are shown in Figs. 5 and 6, while the dependence of the minimum reconstruction error on the full set of potential parameters is presented in Fig. 7.

[5]https://github.com/lesgourg/class_public.

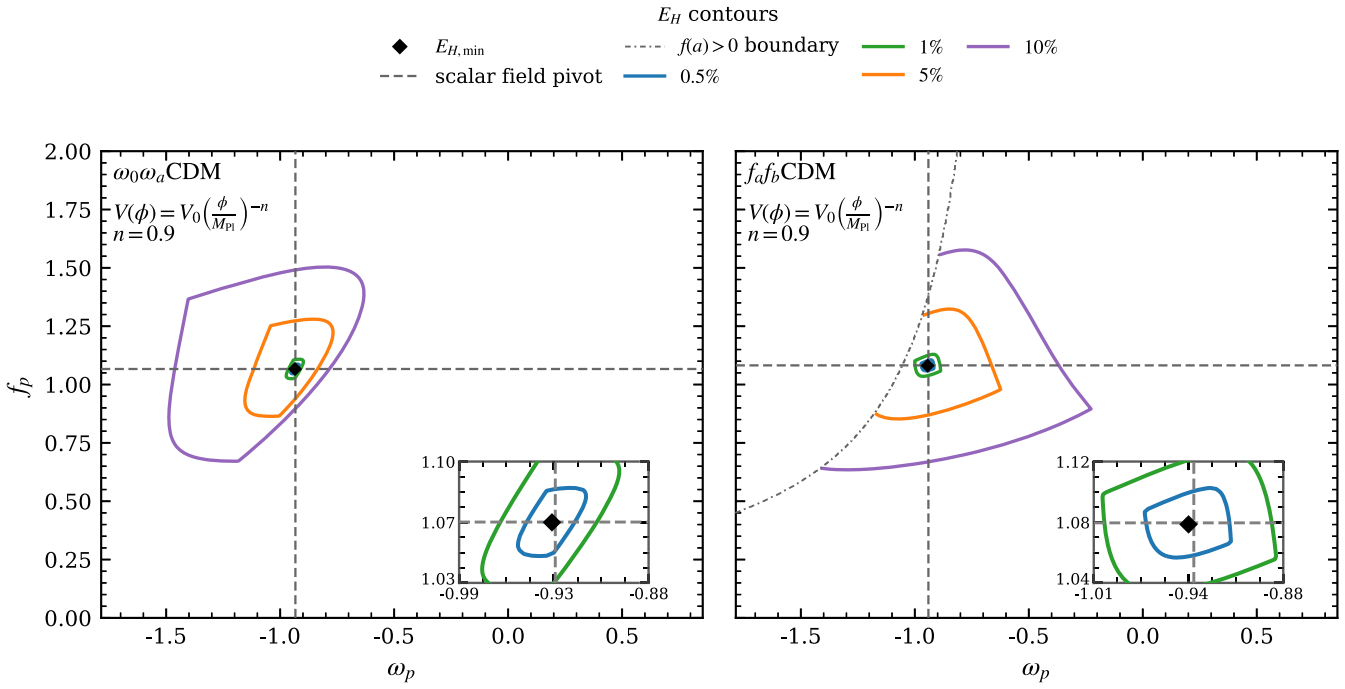


FIG. 6. Same as Fig. 5, but for the Ratra–Peebles inverse power-law potential $V(\phi) = V_0(\phi/M_{\rm Pl})^{-n}$ with $n = 0.9$. The left panel shows the pivoted $\omega_0\omega_a$CDM reconstruction and the right panel the $f_a f_b$CDM reconstruction. The black diamonds identify the continuously optimized minima of E_H, while the dashed gray lines indicate the exact scalar field quantities $\omega_\phi(a_p)$ and $f_\phi(a_p)$ at the corresponding pivot epochs. The gray dot-dashed line in the $f_a f_b$CDM panel delimits the globally physical region satisfying $f(a) > 0$ for every $0 < a \leq 1$.

For each scalar field background, whose Hubble rate is denoted by $H_\phi(z)$, we compare its expansion history with those reconstructed using the pivoted $\omega_0\omega_a$CDM and $f_a f_b$CDM parametrizations. The contours shown in Figs. 5 and 6 describe the accuracy of the reconstructed expansion history and do not correspond to MCMC confidence regions. The MCMC analysis enters only through the determination of the corresponding pivot scale factors a_p, as described in Sec. III.

The reconstruction accuracy for each pair (ω_p, f_p) is quantified through the maximum relative deviation,

$$E_H(\omega_p, f_p) = \max_{z\in[0,4]} \left| \frac{H_{\rm fit}(z) - H_\phi(z)}{H_\phi(z)} \right|, \tag{55}$$

where $H_{\rm fit}(z)$ denotes the Hubble rate predicted by the parametrization under consideration. Here, the quantity $E_H(\omega_p, f_p)$ is evaluated across the (ω_p, f_p) plane, and the contours in Figs. 5 and 6 correspond to the fixed values $E_H = 0.5\%$, 1%, 5%, and 10%. The black diamonds mark the parameter values for which the reconstruction error reaches its minimum.

The upper limit $z = 4$ approximately covers the redshift interval over which current BAO and supernovae observations constrain the late time expansion history.

The pivot epochs are not chosen arbitrarily. For each parametrization, they are inferred from the corresponding weighted MCMC posterior, as discussed in Sec. III. Both parametrizations are then expressed in terms of the physical quantities (ω_p, f_p) evaluated at their respective pivot epochs.

For the exponential model with $\lambda = 0.7$, the continuously optimized minimum errors are

$$E_{H,\min}^{\omega_0\omega_a{\rm CDM}} \simeq 1.3 \times 10^{-4}, \tag{56a}$$

$$E_{H,\min}^{f_a f_b{\rm CDM}} \simeq 1.8 \times 10^{-4}. \tag{56b}$$

These values correspond to maximum relative differences in the Hubble rate of approximately 0.013% and 0.018%, respectively. Both parametrizations reproduce the scalar field background well below the 0.1% level, although the pivoted $\omega_0\omega_a$CDM reconstruction reaches the smaller minimum for this benchmark.

The contour areas provide information complementary to the absolute minimum. We compare them within the common domain,

$$-3 \leq \omega_p \leq 1, \qquad 10^{-3} \leq f_p \leq 2, \tag{57}$$

using the coordinate measure $d\omega_p df_p$. For $f_a f_b$CDM, the area is restricted to the globally physical region satisfying $f(a) > 0$ for every $0 < a \leq 1$.

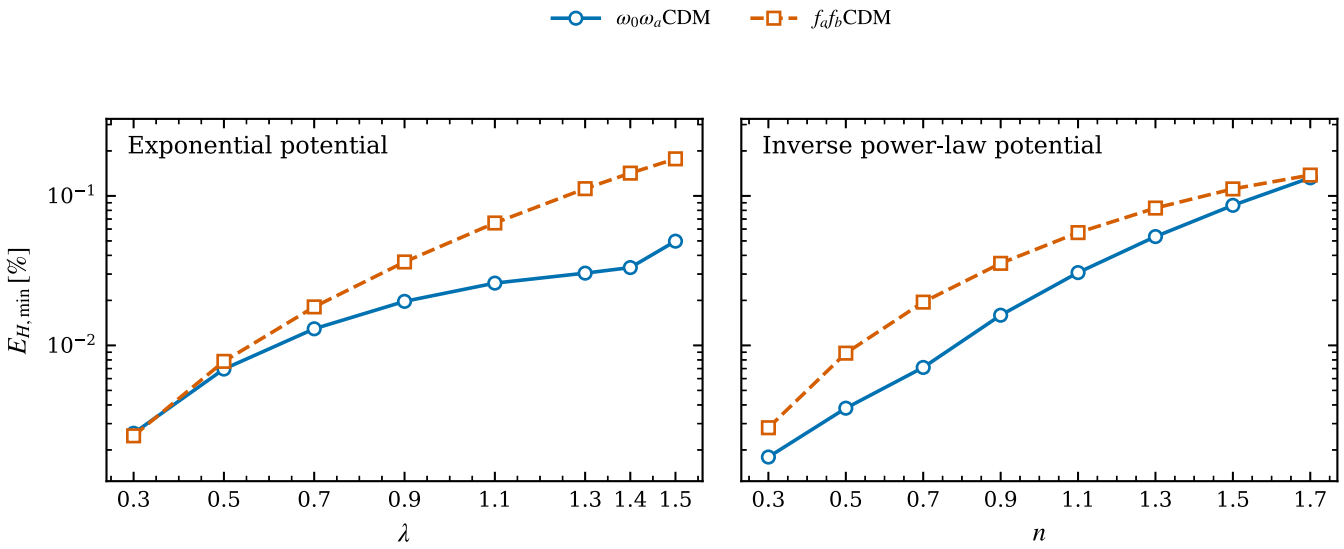


FIG. 7. Continuously optimized minimum Hubble rate reconstruction error for the exponential and Ratra–Peebles quintessence families. The left panel shows $E_{H,\min}$ as a function of the exponential slope λ, while the right panel shows the corresponding result as a function of the inverse power-law exponent n. The vertical axis shows $E_{H,\min}$ in percent. Both panels use the same logarithmic scale. For f_af_bCDM, the optimization is restricted to the globally physical domain satisfying $f(a) > 0$ for every $0 < a \leq 1$. The pivoted $\omega_0\omega_a$CDM reconstruction reaches the lower minimum for almost all the backgrounds considered. The only exception is the exponential potential with $\lambda = 0.3$, for which the difference between the two minimum errors is numerically small.

For the exponential benchmark, the ratios between the f_af_bCDM and pivoted CPL areas are

$$\frac{\mathcal{A}_{f_af_b}}{\mathcal{A}_{\mathrm{CPL}}} \simeq (2.04, 2.02, 1.43, 1.08), \tag{58}$$

for the 0.5%, 1%, 5%, and 10% thresholds, respectively. Thus, in the adopted pivot coordinates and prior domain, the pivoted CPL reconstruction selects a more localized region of parameter space.

We next consider the Ratra–Peebles potential with $n = 0.9$, displayed in Fig. 6. In this case, the minimum errors are

$$E_{H,\min}^{\omega_0\omega_a\mathrm{CDM}} \simeq 1.6 \times 10^{-4}, \tag{59a}$$

$$E_{H,\min}^{f_af_b\mathrm{CDM}} \simeq 3.5 \times 10^{-4}. \tag{59b}$$

The corresponding maximum deviations are approximately 0.016% and 0.035%. Both reconstructions again remain below the 0.1% level, but the minimum obtained with pivoted CPL is smaller by a factor of approximately 2.22.

For this inverse power-law benchmark, the corresponding contour area ratios are

$$\frac{\mathcal{A}_{f_af_b}}{\mathcal{A}_{\mathrm{CPL}}} \simeq (2.13, 2.07, 1.50, 1.12), \tag{60}$$

again for the 0.5%, 1%, 5%, and 10% thresholds. The pivoted CPL contours are therefore more compact for this representative Ratra–Peebles model as well.

The contour area comparison should be interpreted within the specific coordinates and prior domain adopted here. In particular, an area measured using $d\omega_p df_p$ is not invariant under a nonlinear redefinition of the parameters. The ratios in Eqs. (58) and (60) should therefore not be regarded as absolute parameter volume measures. They quantify the relative extension of the accuracy regions only after both models have been placed in the same pivot coordinates.

This comparison differs from the usual one between the original (ω_0, ω_a) CPL basis and a pivoted density-level parametrization [88]. The elongated structures commonly associated with CPL are strongly influenced by the correlation between ω_0 and ω_a. Expressing CPL instead through (ω_p, f_p) substantially reduces this degeneracy and produces compact accuracy contours. Consequently, the compactness found for a density-level parametrization cannot be interpreted independently of the parameter basis used in the comparison.

The dashed lines in Figs. 5 and 6 mark the exact values of $\omega_\phi(a_p)$ and $f_\phi(a_p)$ obtained from the numerical scalar field solution. Their intersection provides a direct reference for comparing the effective parameters that minimize E_H with the physical dark energy properties at the corresponding pivot epoch. This is a separate requirement from minimizing the discrepancy in $H(z)$; i.e., because the Hubble rate depends on the expansion history, the parameters yielding the smallest E_H need not coincide exactly with the instantaneous scalar field quantities at a_p.

The complete set of continuously optimized minimum errors is summarized in Fig. 7.

The pivoted $\omega_0\omega_a$CDM model gives the smaller $E_{H,\min}$ among all the scalar field backgrounds, with the only exception of $\lambda = 0.3$ in the exponential potential, for which

$$E_{H,\min}^{\omega_0\omega_a\mathrm{CDM}} \simeq 2.6 \times 10^{-5}, \tag{61a}$$

$$E_{H,\min}^{f_a f_b\mathrm{CDM}} \simeq 2.5 \times 10^{-5}. \tag{61b}$$

The absolute difference between the two minima is only approximately 1.0×10^{-6} in E_H.

Therefore, this isolated case does not indicate a substantial difference in reconstruction accuracy.

Nevertheless, all the reconstructed backgrounds remain accurate over $0 \leq z \leq 4$.

The relative advantage of pivoted CPL is most evident for intermediate and larger values of the exponential slope, while for the inverse power-law family the difference gradually decreases again toward the largest sampled values of n.

Overall, the two parametrizations both provide accurate effective descriptions of the scalar field expansion histories. Within the adopted error measure, prior domain, and pivot coordinates, the pivoted $\omega_0\omega_a$CDM parametrization reaches the smaller optimized error in nearly all the cases and also produces more compact fixed accuracy regions for the two displayed benchmarks. These results show that the performance of a dark energy parametrization depends not only on whether it is constructed from $\omega(a)$ or from the density evolution but also on the variables used to express it and on the underlying scalar field dynamics.

V. FINAL OUTLOOKS AND PERSPECTIVES

In this work, we investigated the role of parameter coordinates in describing dark energy evolution. Motivated by the recent DESI results and by the renewed interest in possible departures from the cosmological constant, we compared the standard $\omega_0\omega_a$CDM model with a generic $f_a f_b$CDM parametrization, where normalized dark energy density is described through a second order Taylor expansion around the present epoch.

This scenario emulates the $\omega_0\omega_a$CDM model changing the expansion directly on dark energy density, with the purpose of understanding whether this choice may turn into an advantage in the dark energy reconstruction. We thus checked if choosing a different Taylor expansion arose from the parameter basis used to represent the same background information.

To do so, we first reviewed the standard pivot construction for the $\omega_0\omega_a$CDM model and then extended the pivot technique to a density-level pair, defined by the equation of state and the normalized dark energy density evaluated at an optimized pivot epoch. For CPL, the transformation represented an alternative setup of the well-known expansion that did not alter the expansion history, the likelihood, or the physical content of the cosmology. In particular, the same pivot variables were then reconstructed for the $f_a f_b$CDM model, allowing the two parametrizations to be compared in a common physical coordinate system.

This procedure allowed us to separate two mixed effects in optimizing dark energy reconstructions. Precisely, the first lies on the actual choice of the model, namely, whether one expands the equation of state or the dark energy density, whereas the second is the choice of coordinates used to display and constrain the posterior. We showed that the parametrization may appear more stable or less degenerate simply because it is written in a better basis, namely, when the choice of Taylor expansion matches the directions selected by the data, minimizing the correlation between parameters.

We constrained both models using a combination of CMB compressed data, DESI DR2 BAO measurements, cosmic chronometer data, Pantheon + Type Ia supernovae, and the SH0ES prior on H_0. In the original parameter bases, the CPL model gave a slightly lower minimum chi-square than the $f_a f_b$CDM model for the dataset combination adopted in this work. The inferred values of H_0 and Ω_{m} were very close in the two parametrizations, showing that the main differences appeared in the dark energy sector rather than in the standard background parameters.

The pivot analysis then showed that the density-level pivot construction worked particularly well for CPL. In the CPL case, the optimized pivot epoch led to an effectively decorrelated pair of physical dark energy variables. Conversely, in the $f_a f_b$CDM case the same procedure reduced the original strong degeneracy between the density expansion coefficients, without removing the residual correlation completely. The original f_a and f_b parameters were highly anticorrelated, while the pivoted variables displayed a much milder correlation. Nevertheless, the decorrelation was more complete in the pivoted CPL basis.

The pivoted constraints also showed that both parametrizations selected a mildly phantom value of the dark energy equation of state at the pivot epoch, while the normalized dark energy density remained close to unity. This indicated that the deviation from the cosmological constant appeared mainly through the local slope of the reconstructed dark energy evolution. Accordingly, the CPL result tends to be closer to the ΛCDM model, reopening the debate toward the validity of DESI results. Nevertheless, the density expansion showed a somewhat stronger phantom tendency in the pivoted variables.

We further tested the two pivoted parametrizations against canonical quintessence models described by an exponential potential and by a Ratra–Peebles inverse power-law potential. This comparison was introduced as an independent validation of the ability of the two phenomenological forms to reproduce a smooth scalar field background that was not generated by either ansatz.

The scalar field evolution was computed numerically with `CLASS`, and the reconstructed Hubble histories were compared over the redshift range relevant for late time probes.

Both parametrizations reproduced the quintessence background with high accuracy. However, for the benchmark model considered here, the pivoted CPL parametrization reached the smallest maximum relative deviation in the Hubble rate. It also selected a more compact region of the physical parameter plane for fixed reconstruction accuracy and recovered more closely the exact scalar field values of the equation of state and normalized density at the corresponding pivot epoch. The $f_a f_b$CDM model showed minimum error regions that appear broader and more displaced from the exact quintessence values.

Hence, we conclude that a significant part of the improvement associated with the $f_a f_b$CDM basis was traced to the use of a more favorable coordinate system. Once the same density-level pivot logic was applied to the $\omega_0\omega_a$CDM model, the physical pivot variables became effectively uncorrelated, while the reconstructed scalar field backgrounds were reproduced more accurately in nearly all the cases considered than with the density Taylor expansion.

Consequently, the strength of departures from the standard cosmological model depends on the coordinates used to describe the posterior. For this reason, claims of dynamical dark energy should be tested also against physically motivated reparametrizations of the same model.

As future works, several extensions of the analysis appear natural. The comparison with scalar field dynamics should be repeated for a wider set of quintessence potentials, including additional thawing and freezing models, other tracker solutions, and dark energy histories with sharper transitions. The stability of the pivot epoch should also be tested under different dataset combinations, especially by comparing analyses with and without the SH0ES prior and by replacing compressed CMB information with full temperature, polarization, and lensing likelihoods. A consistent treatment of dark energy perturbations will also be included in this extension. Finally, the role of priors under nonlinear changes of variables should be studied more systematically, since the likelihood remains unchanged under reparametrization whereas the posterior may depend on the chosen prior measure.

ACKNOWLEDGMENTS

Y. C. and O. L. acknowledge the financial support provided by the Brera Astronomical Observatory of the National Institute for Astrophysics (INAF), and the hospitality of the National Centre for Nuclear Research (NCBJ), Warsaw, where this work was carried out. They are also very grateful to Anna Chiara Alfano, Gabriele Montefalcone, and Bharat Ratra for insightful discussions on the topic of pivot and dark energy evolution. M. B. was supported by the Polish National Science Centre Grant No. 2023/50/A/ST9/00579.

DATA AVAILABILITY

The observational datasets and software packages used in this analysis are publicly available through the references and repositories cited in the manuscript. Additional information and analysis products may be obtained from the authors upon reasonable request.

[1] G. Gu *et al.* (DESI Collaboration), Nat. Astron. **9**, 1879 (2025); **9**, 1898(E) (2025).
[2] Y. Tada and T. Terada, Phys. Rev. D **109**, L121305 (2024).
[3] I. D. Gialamas, G. Hütsi, K. Kannike, A. Racioppi, M. Raidal, M. Vasar, and H. Veermäe, Phys. Rev. D **111**, 043540 (2025).
[4] W. Giarè, M. Najafi, S. Pan, E. Di Valentino, and J. T. Firouzjaee, J. Cosmol. Astropart. Phys. 10 (2024) 035.
[5] O. Luongo and H. Quevedo, Phys. Rev. D **90**, 084032 (2014).
[6] O. Luongo and H. Quevedo, in *12th Marcel Grossmann Meeting on General Relativity* (2010), pp. 1029–1031, arXiv:1005.4532.
[7] A. G. Riess *et al.* (Supernova Search Team Collaboration), Astron. J. **116**, 1009 (1998).
[8] S. Perlmutter *et al.* (Supernova Cosmology Project Collaboration), Astrophys. J. **517**, 565 (1999).
[9] E. J. Copeland, M. Sami, and S. Tsujikawa, Int. J. Mod. Phys. D **15**, 1753 (2006).
[10] S. M. Carroll, Living Rev. Relativity **4**, 1 (2001).
[11] P. J. E. Peebles and B. Ratra, Rev. Mod. Phys. **75**, 559 (2003).
[12] J. Frieman, M. Turner, and D. Huterer, Annu. Rev. Astron. Astrophys. **46**, 385 (2008).
[13] V. Sahni, Lect. Notes Phys. **653**, 141 (2004).
[14] T. Padmanabhan, AIP Conf. Proc. **861**, 179 (2006).
[15] R. R. Caldwell and M. Kamionkowski, Annu. Rev. Nucl. Part. Sci. **59**, 397 (2009).
[16] A. C. Alfano, O. Luongo, and M. Muccino, J. High Energy Astrophys. **46**, 100348 (2025).
[17] O. Luongo and M. Muccino, Astron. Astrophys. **693**, A187 (2025).
[18] A. C. Alfano and O. Luongo, Phys. Dark Universe **51**, 102205 (2026).

[19] K. Boshkayev, T. Konysbayev, O. Luongo, M. Muccino, and F. Pace, Phys. Rev. D **104**, 023520 (2021).
[20] P. K. S. Dunsby, O. Luongo, and M. Muccino, Phys. Rev. D **109**, 023510 (2024).
[21] A. C. Alfano, O. Luongo, and M. Muccino, J. Cosmol. Astropart. Phys. 12 (2024) 055.
[22] O. Luongo and M. Muccino, Mon. Not. R. Astron. Soc. **518**, 2247 (2022).
[23] A. C. Alfano, S. Capozziello, O. Luongo, and M. Muccino, J. High Energy Astrophys. **42**, 178 (2024).
[24] Y. Carloni and O. Luongo, Classical Quantum Gravity **42**, 075014 (2025).
[25] P. K. S. Dunsby, O. Luongo, and L. Reverberi, Phys. Rev. D **94**, 083525 (2016).
[26] M. Muccino, L. Izzo, O. Luongo, K. Boshkayev, L. Amati, M. Della Valle, G. B. Pisani, and E. Zaninoni, Astrophys. J. **908**, 181 (2021).
[27] D. H. Weinberg, M. J. Mortonson, D. J. Eisenstein, C. Hirata, A. G. Riess, and E. Rozo, Phys. Rep. **530**, 87 (2013).
[28] N. Aghanim *et al.* (Planck Collaboration), Astron. Astrophys. **641**, A6 (2020); **652**, C4(E) (2021).
[29] S. Alam *et al.* (eBOSS Collaboration), Phys. Rev. D **103**, 083533 (2021).
[30] T. M. C. Abbott *et al.* (DES Collaboration), Phys. Rev. D **105**, 023520 (2022).
[31] D. Brout *et al.*, Astrophys. J. **938**, 110 (2022).
[32] D. Huterer and D. L. Shafer, Rep. Prog. Phys. **81**, 016901 (2018).
[33] D. N. Spergel *et al.* (WMAP Collaboration), Astrophys. J. Suppl. Ser. **148**, 175 (2003).
[34] M. Tegmark *et al.* (SDSS Collaboration), Phys. Rev. D **69**, 103501 (2004).
[35] S. Alam *et al.* (BOSS Collaboration), Mon. Not. R. Astron. Soc. **470**, 2617 (2017).
[36] V. Sahni and A. A. Starobinsky, Int. J. Mod. Phys. D **09**, 373 (2000).
[37] J. Martin, C.R. Phys. **13**, 566 (2012).
[38] I. Zlatev, L.-M. Wang, and P. J. Steinhardt, Phys. Rev. Lett. **82**, 896 (1999).
[39] H. E. S. Velten, R. F. vom Marttens, and W. Zimdahl, Eur. Phys. J. C **74**, 3160 (2014).
[40] C. P. Burgess, in *100e Ecole d'Ete de Physique: Post-Planck Cosmology* (2015), pp. 149–197, arXiv:1309.4133.
[41] S. Nobbenhuis, Found. Phys. **36**, 613 (2006).
[42] N. Dalal, K. Abazajian, E. E. Jenkins, and A. V. Manohar, Phys. Rev. Lett. **87**, 141302 (2001).
[43] O. Luongo and H. Quevedo, Int. J. Mod. Phys. D **23**, 1450012 (2014).
[44] O. Luongo and M. Muccino, Phys. Rev. D **98**, 103520 (2018).
[45] A. Belfiglio, Y. Carloni, and O. Luongo, Phys. Dark Universe **44**, 101458 (2024).
[46] S. Weinberg, Rev. Mod. Phys. **61**, 1 (1989).
[47] H. Martel, P. R. Shapiro, and S. Weinberg, Astrophys. J. **492**, 29 (1998).
[48] S. Weinberg, in *Sources and Detection of Dark Matter and Dark Energy in the Universe* (Springer, Berlin, Heidelberg, 2001), pp. 18–26.
[49] T. Padmanabhan, Phys. Rep. **380**, 235 (2003).
[50] R.-G. Cai and S.-J. Wang, Res. Astron. Astrophys. **26**, 084011 (2026).
[51] E. Di Valentino, O. Mena, S. Pan, L. Visinelli, W. Yang, A. Melchiorri, D. F. Mota, A. G. Riess, and J. Silk, Classical Quantum Gravity **38**, 153001 (2021).
[52] Y. Carloni, O. Luongo, and M. Muccino, Astron. Astrophys. **707**, A383 (2026).
[53] Y. Carloni and O. Luongo, arXiv:2604.18053.
[54] Y. Carloni, Int. J. Mod. Phys. A **41**, 2646023 (2026).
[55] I. Pantos and L. Perivolaropoulos, Phys. Dark Universe **52**, 102286 (2026).
[56] A. G. Adame *et al.* (DESI Collaboration), J. Cosmol. Astropart. Phys. 02 (2025) 021.
[57] M. Abdul Karim *et al.* (DESI Collaboration), Phys. Rev. D **112**, 083515 (2025).
[58] K. Lodha *et al.* (DESI Collaboration), Phys. Rev. D **112**, 083511 (2025).
[59] T.-N. Li, G.-H. Du, S.-H. Zhou, Y.-H. Li, J.-F. Zhang, and X. Zhang, Phys. Dark Universe **52**, 102254 (2026).
[60] T.-N. Li, G.-H. Du, H. Wang, Y.-H. Li, J.-F. Zhang, and X. Zhang, Res. Astron. Astrophys. **26**, 084002 (2026).
[61] A. Chudaykin and M. Kunz, Phys. Rev. D **110**, 123524 (2024).
[62] W. J. Wolf, C. García-García, and P. G. Ferreira, J. Cosmol. Astropart. Phys. 05 (2025) 034.
[63] M. Vincenzi *et al.* (DES Collaboration), Mon. Not. R. Astron. Soc. **541**, 2585 (2025).
[64] A. Paliathanasis, Phys. Dark Universe **48**, 101956 (2025).
[65] A. Paliathanasis, J. Cosmol. Astropart. Phys. 09 (2025) 067.
[66] Z. Lu, T. Simon, and P. Zhang, arXiv:2503.04602.
[67] A. Paliathanasis, arXiv:2605.30139.
[68] A. Paliathanasis, Phys. Dark Universe **52**, 102306 (2026).
[69] O. Luongo and M. Muccino, Astron. Astrophys. **690**, A40 (2024).
[70] Y. Carloni, O. Luongo, and M. Muccino, Phys. Rev. D **111**, 023512 (2025).
[71] G. Efstathiou, Mon. Not. R. Astron. Soc. **538**, 875 (2025).
[72] G. Efstathiou, Mon. Not. R. Astron. Soc. **540**, 2844 (2025).
[73] S. Afroz and S. Mukherjee, Phys. Rev. D **113**, 083514 (2026).
[74] R. de Souza, A. Sousa-Neto, J. E. González, and J. Alcaniz, Phys. Rev. D **113**, 103531 (2026).
[75] E. Ó. Colgáin and M. M. Sheikh-Jabbari, Mon. Not. R. Astron. Soc. **542**, L24 (2025).
[76] E. Ó. Colgáin, M. G. Dainotti, S. Capozziello, S. Pourojaghi, M. M. Sheikh-Jabbari, and D. Stojkovic, J. High Energy Astrophys. **49**, 100428 (2026).
[77] E. Ó. Colgáin, S. Pourojaghi, and M. M. Sheikh-Jabbari, Galaxies **13**, 133 (2025).
[78] E. Ó. Colgáin, S. Pourojaghi, M. M. Sheikh-Jabbari, and L. Yin, Phys. Dark Universe **52**, 102268 (2026).
[79] R. E. Keeley, K. N. Abazajian, M. Kaplinghat, and A. Shafieloo, Phys. Rev. D **112**, 043501 (2025).
[80] A. Sousa-Neto, C. Bengaly, J. E. Gonzalez, and J. Alcaniz, Phys. Dark Universe **50**, 102108 (2025).
[81] M. Chevallier and D. Polarski, Int. J. Mod. Phys. D **10**, 213 (2001).

[82] D. Huterer and M. S. Turner, Phys. Rev. D **64**, 123527 (2001).
[83] E. V. Linder, Phys. Rev. Lett. **90**, 091301 (2003).
[84] A. Albrecht *et al.*, arXiv:astro-ph/0609591.
[85] E. V. Linder, Astropart. Phys. **26**, 102 (2006).
[86] W. Yang, S. Pan, E. Di Valentino, and E. N. Saridakis, Universe **5**, 219 (2019).
[87] M. Cortês and A. R. Liddle, J. Cosmol. Astropart. Phys. 12 (2024) 007.
[88] G. Montefalcone and R. Stiskalek, Phys. Rev. D **114**, 043538 (2026).
[89] D. Huterer and A. Cooray, Phys. Rev. D **71**, 023506 (2005).
[90] Y. Wang and K. Freese, Phys. Lett. B **632**, 449 (2006).
[91] https://github.com/LauraHerold/MontePython_desilike.
[92] R. Jimenez and A. Loeb, Astrophys. J. **573**, 37 (2002).
[93] C. Zhang, H. Zhang, S. Yuan, T.-J. Zhang, and Y.-C. Sun, Res. Astron. Astrophys. **14**, 1221 (2014).
[94] J. Simon, L. Verde, and R. Jimenez, Phys. Rev. D **71**, 123001 (2005).
[95] M. Moresco *et al.*, J. Cosmol. Astropart. Phys. 08 (2012) 006.
[96] M. Moresco, L. Pozzetti, A. Cimatti, R. Jimenez, C. Maraston, L. Verde, D. Thomas, A. Citro, R. Tojeiro, and D. Wilkinson, J. Cosmol. Astropart. Phys. 05 (2016) 014.
[97] A. L. Ratsimbazafy, S. I. Loubser, S. M. Crawford, C. M. Cress, B. A. Bassett, R. C. Nichol, and P. Väisänen, Mon. Not. R. Astron. Soc. **467**, 3239 (2017).
[98] D. Stern, R. Jimenez, L. Verde, M. Kamionkowski, and S. A. Stanford, J. Cosmol. Astropart. Phys. 02 (2010) 008.
[99] N. Borghi, M. Moresco, and A. Cimatti, Astrophys. J. Lett. **928**, L4 (2022).
[100] M. Moresco, Mon. Not. R. Astron. Soc. **450**, L16 (2015).
[101] A. G. Riess *et al.*, Astrophys. J. Lett. **934**, L7 (2022).
[102] G. Alestas, D. Camarena, E. Di Valentino, L. Kazantzidis, V. Marra, S. Nesseris, and L. Perivolaropoulos, Phys. Rev. D **105**, 063538 (2022).
[103] M. Kamionkowski and A. G. Riess, Annu. Rev. Nucl. Part. Sci. **73**, 153 (2023).
[104] Z. Zhou, Z. Miao, S. Bi, C. Ai, and H. Zhang, Phys. Rev. D **112**, 103502 (2025).
[105] Y. Carloni, O. Luongo, and M. Biesiada, Phys. Rev. D **113**, 103525 (2026).
[106] M. Kunz, R. Trotta, and D. Parkinson, Phys. Rev. D **74**, 023503 (2006).
[107] N. Sugiura, Commun. Stat., Theory Methods **7**, 13 (1978).
[108] M. Biesiada, J. Cosmol. Astropart. Phys. 02 (2007) 003.
[109] M. Szydlowski, T. Stachowiak, and R. Wojtak, Phys. Rev. D **73**, 063516 (2006).
[110] M. Szydlowski and A. Kurek, AIP Conf. Proc. **861**, 1031 (2006).
[111] A. Melchiorri, L. Pagano, and S. Pandolfi, Phys. Rev. D **76**, 041301 (2007).
[112] S. Capozziello, P. K. S. Dunsby, and O. Luongo, Mon. Not. R. Astron. Soc. **509**, 5399 (2021).
[113] A. C. Alfano, C. Cafaro, S. Capozziello, and O. Luongo, Phys. Dark Universe **42**, 101298 (2023).
[114] J. V. Cunha and J. A. S. Lima, Mon. Not. R. Astron. Soc. **390**, 210 (2008).
[115] O. Farooq and B. Ratra, Astrophys. J. Lett. **766**, L7 (2013).
[116] M. Vargas dos Santos, R. R. R. Reis, and I. Waga, J. Cosmol. Astropart. Phys. 02 (2016) 066.
[117] M. Muccino, O. Luongo, and D. Jain, Mon. Not. R. Astron. Soc. **523**, 4938 (2023).
[118] R. R. Caldwell and E. V. Linder, Phys. Rev. Lett. **95**, 141301 (2005).
[119] R. J. Scherrer and A. A. Sen, Phys. Rev. D **77**, 083515 (2008).
[120] E. J. Copeland, A. R. Liddle, and D. Wands, Phys. Rev. D **57**, 4686 (1998).
[121] O. F. Ramadan, J. Sakstein, and D. Rubin, Phys. Rev. D **110**, L041303 (2024).
[122] M. W. Toomey, G. Montefalcone, E. McDonough, and K. Freese, Phys. Rev. D **113**, 123532 (2026).
[123] B. Ratra and P. J. E. Peebles, Phys. Rev. D **37**, 3406 (1988).
[124] P. J. Steinhardt, L.-M. Wang, and I. Zlatev, Phys. Rev. D **59**, 123504 (1999).